Current Biology, Volume *24*

Supplemental Information

Neural Pathways for the Detection and Discrimination of Conspecific Song in *D. melanogaster*

Alexander G. Vaughan, Chuan Zhou, Devanand S. Manoli, and Bruce S. Baker

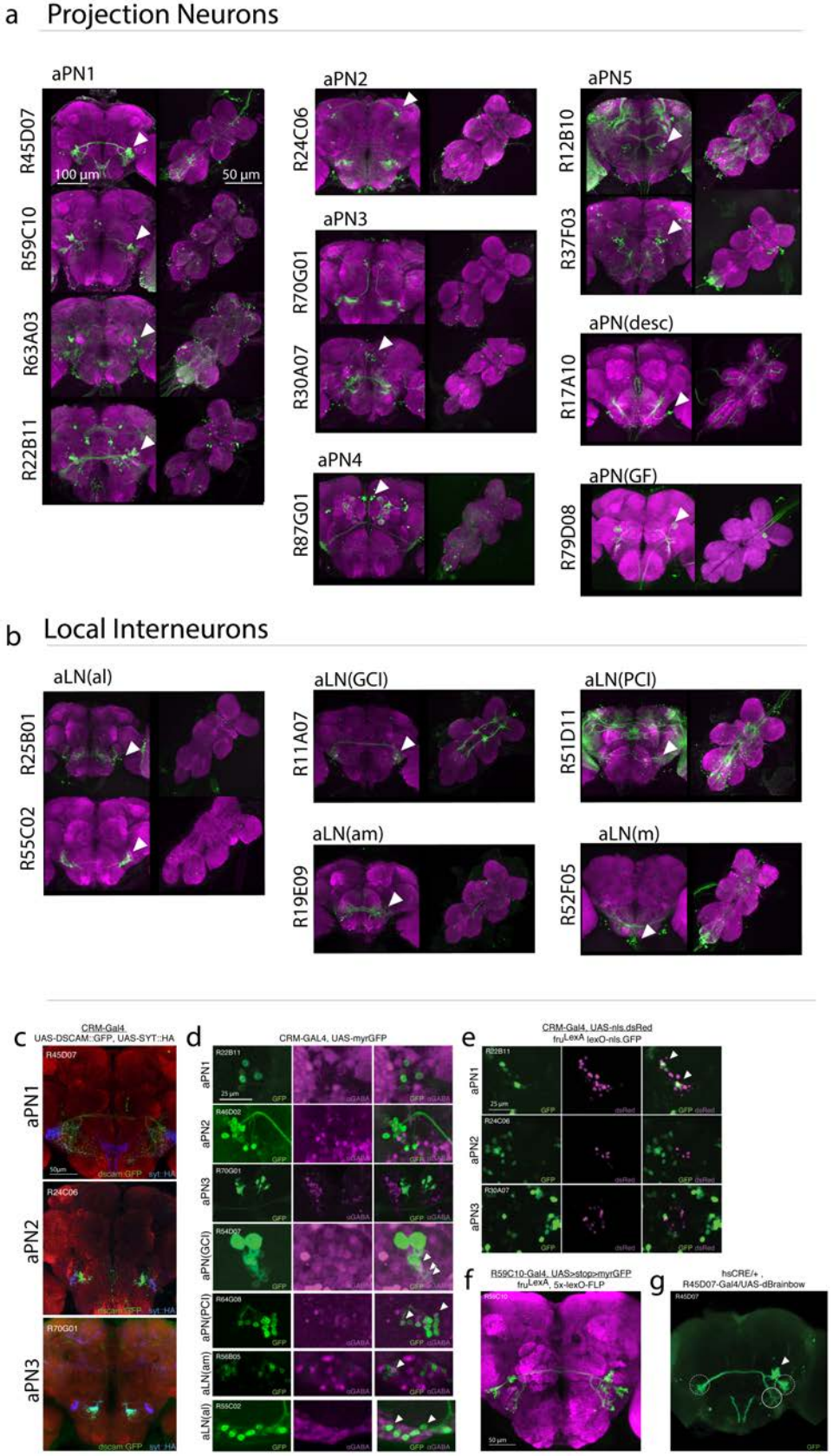
a Projection Neurons
aPN1
R45D07
R59C10
R63A03
R22B11
100 µm
50 µm
aPN2
R24C06
aPN3
R70G01
R30A07
aPN4
R87G01
aPN5
R12B10
R37F03
aPN(desc)
R17A10
aPN(GF)
R79D08
b Local Interneurons
aLN(al)
R25B01
R55C02
aLN(GCI)
R11A07
aLN(PCI)
R51D11
aLN(am)
R19E09
aLN(m)
R52F05
c
CRM-Gal4,
UAS-DSCAM::GFP, UAS-SYT::HA
aPN1
aPN2
aPN3
dscam:GFP
syt::HA
d
CRM-GAL4, UAS-myrGFP
aPN1
aPN2
aPN3
aPN(GCI)
aPN(PCI)
aLN(am)
aLN(al)
GFP
αGABA
e
CRM-Gal4, UAS-nls.dsRed
fruLexA lexO-nls.GFP
aPN1
aPN2
aPN3
GFP
dsRed
f
R59C10-Gal4, UAS>stop>myrGFP
fruLexA, 5x-lexO-FLP
g
hsCRE/+ ,
R45D07-Gal4/UAS-dBrainbow

Figure S1, related to Figure 1. a-b Expression pattern of CRM-GAL4 lines for each aPN and aLN cell type**. a-b** CRM lines for each putative aPN (**a)** and aLN (**b**) cell type are shown, driving the expression of GFP from pJFRC-2 in male flies. Maximum-intensity Z-stacks are shown for each brain and VNC, normalized to show the full range of GFP expression without saturation. Cell bodies are identified with a white triangle. **c-g** Anatomy and gene expression in aPNs and aLNs. **c** Visualization of dendritic and axonal fields in WED-innervating aPNs by expression of pre-synaptic (DSCAM::GFP) and post-synaptic (SYT::HA) epitope tags in female flies. Neurons expressing these tags in aPN1 (R22B11) and aPN2 (R24C06) show GFP staining in the AMMC alone, and HA staining in the WED alone. Under the aPN3 driver R70G01, GFP is visible in the AMMC while HA staining is visible in both AMMC and WED, suggesting bidirectional outputs. **d** Expression of GABA in novel aPNs projecting to the WED. No GABAergic expression was observed in aPN1, aPN2, or aPN3 cell types in female flies, but GABA was visible in at least a subset of all aLN populations. **e** Expression of fru^{M} in novel aPNs projecting to the WED. Expression of a fru^{M} transcriptional reporter was observed in aPN1 in male flies, but not in aPN2 or aPN3. **f** Arborization of fru^{M}-expressing aPN1 neurons in male flies. Expression of R59C10 was visualized by *flp*-mediated intersection with fru^{LexA}; the projection pattern of this subset largely matches the canonical projection of aPN1a,b neurons (Table S2). **g** Unilateral aPN1 clone from 45D07: Brainbow in female flies. aPN1 neurons arising from the left hemisphere are labeled by GFP expression from dBrainbow. This cell type innervates AMMC (circle, solid)

ipsilaterally to the cell bodies (arrow) and innervates WED bilaterally (circle, dashed).

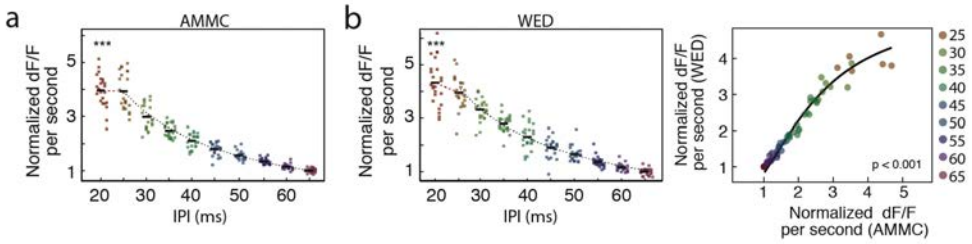

Figure S2, related to Figure 7. GCaMP response of aPN1 to pulse song, shown as *ΔF/F per second of stimulus* **a-c** One potential concern with the GCaMP technique is that finite-duration sampling may introduce artifacts into the GCaMP response. The stimuli used here were restricted to 40 pulses, to avoid the apparent effect of aPN1 habituation. However, as the apparent integration time of GCaMP3 in *Drosophila* is of the same order as the stimulus duration the peak ΔF/F signal may underestimate the instantaneous GCaMP response at short IPIs (GCaMP time to half max: ~1.5s; stimulus duration: 0.8-2.6s for 20ms-65ms IPI). To compensate for this, we divided the normalized peak ΔF/F signal by the stimulus duration, to generate a metric of ΔF/F per second or the "instantaneous response". **a** The instantaneous response of aPN1 in the dendritic field increases hyperbolically with pulse rate between 25ms and 65ms IPI (AMMC : $R^2 = 0.87$, $p<0.001$ vs. linear fit), with a marked depression of the expected response at 20ms IPI ($p<10^{-4}$ vs. expected value from hyperbolic fit. **b** The instantaneous response rate in WED shows a similar hyperbolic shape between 25ms and 65ms IPI ($R^2 = 0.88$, $p<0.03$ vs. linear fit) as well as a depression 20ms IPI ($p<10^{-4}$ vs. expected value from hyperbolic fit). **c** The input-output dynamics of AMMC and WED responses show a similar nonlinear damping process. Pairwise comparison

of ΔF/F per second response in dendritic and axonal fields, normalized by the response at 65ms IPI, shows a nonlinear damping of the axonal response relative to the dendritic response at low IPIs ($R^2 = 0.97$, $p<0.01$ vs. linear fit). Note that the AMMC-WED transfer function was also unchanged, as both AMMC and WED responses are scaled by the same factor at each IPI (Figure 7i).

Projection Neurons		**AMMC Arborization Zone and Projection**			***fru*^{M}**	**GABA**
aPN1	AMMC Projection Neuron 1	B	→	WED	+	-
aPN2	AMMC Projection Neuron 2	C/E	→	WED	–	-
aPN3	AMMC Projection Neuron 3	C/E	⇄	WED	–	-
aPN4	AMMC Projection Neuron 4	A	→	PP	–	
aPN5	AMMC Projection Neuron 5	A	→	PP	+	
aPN(desc)	AMMC Projection Neuron, descending	A/B	→	VNC *contra*	+	
aPN(GF)	AMMC Projection Neuron, Giant Fiber	A	→	VNC *ipsi*		-
Local Interneurons		**AMMC Arborization Zone**			***fru*^{M}**	**GABA**
alN(al)	AMMC Local Neuron (anterolateral)	B			+	+
aLN(am)	AMMC Local Neuron (anteromedial)	C/E			-	+
aLN(m)	AMMC Local Neuron (medial)	A/B			+	+
aLN(PCI)	AMMC Local Neuron (posterior commissural)	A/B			-	+
aLN(GCI)	AMMC Local Neuron (giant commissural)	A			-	+ subset

Table S1, related to Figure 1. Arborization patterns of each candidate auditory intererneuron identified in this work, as well as expression of *fru*^{M} and GABA in at least a subset of each cell population. Correspondence with similar cell types identified previously are listed in Table S2. *AMMC,* antennal mechanosensory and motor center*; VNC,* ventral nerve cord*; WED,* wedge*; PP,* posterior protocerebrum*; contra,* contralateral*; ipsi,* ipsilateral.

	Identified GAL4 drivers			Clonal analyses			Song responsive
Source	**This work.** CRM-GAL4 lines	**Kamikouchi et al., 2009** GAL4 lines.	**Yu et al., 2010** Overlap of fru^{FLP} and fru^{GAL4}	**Cachero et al. 2010** Clonal analysis of fru^{GAL4}	**Lai et al. 2012** Clonal / functional analysis	**Lin et al., 2012** Clonal analysis of lPN lineage	
Projection neurons	**aPN1a,b** bilateral WED	AMMC-B1	-	aDT-e	AMMC-B1a AMMC-B1b	AMMC-2 through AMMC-8	+
	aPN1c contralateral only	-	-	-	AMMC-IVLP PN1	AMMC-10,11	+
	aPN2	-	-	-	-	-	
	aPN3	-	-	-	-	-	
	aPN4	-	-	-	-	-	
	aPN5	-	aDT5	aDT-g	-	-	
	aPN(desc)	-	-	aSG-a	AMMC-VNC PN	-	
	aPN(GF)	(Giant Fiber)	-	-	-	-	+
Local neurons	**aLN(al)**	-	-	pSG-a	AMMC LN	-	
	aLN(am)	-	-	-	-	-	
	aLN(m)	-	-	pSG-d	AMMC-AMMC PN1	-	
	aLN (PCI)	-	-	-	AMMC-IVLP PN2?	-	
	aLN(GCI) canonical GCI	AMMC-A1?	-	-	-	-	+
	aLN(GCI) GABAergic	AMMC-A1?	-	-	AMMC-VLP PN	-	
No correlates	Not observed	AMMC-B2	-	-	-	-	+
	Not observed	-	-	pSG-b	-	-	
	Not observed	-	-	pSG-c	-	-	
	Not observed	-	pIP1	-	-	-	
	Possibly a rare aPN6 subtype.				AMMC-AMMC PN2		
	Suitable drivers for manipulation not found.	-	-	-	-	AMMC1,9	
		-	-	-	AMMC-A2	AMMC12-16	+

Table S2, related to Figure 1. Correspondence of cell-types identified in this work with previous work. Where possible, we have identified the correspondence between cell types presented in this paper and in previous work. For cell types in Cachero et al. and Yu et al. correspondence only addresses putative fru^{M}-

expressing neurons, while those in other works include both *fru*^{M} expressing and non-expressing neurons.

For aPN1 and aLN(GCI), the cell types defined here should be considered a superset of corresponding cell types identified in previous works. For aPN1, we note that AMMC-B1 was first identified as a set of AMMC interneurons projecting from AMMC zone B across the superior oesophageal commissure to WED; however, Lai et al. distinguish this cell type (which shows bilateral projections to WED) from AMMC-IVLP PN1 (which shows contralateral projections only) [S1]. Notably, both cell types arise from the same progenitor, arising from different developmental epochs of the olfactory lPN lineage [S2]. Since these lineage subtypes are essentially indistinguishable when co-expressed, and are likely both present in the drivers used here, we refer to these as aPN1. However, as we were able to specifically reject drivers that showed expression in more obviously distinct cell types in the lPN lineage (such as AMMC-14 through AMMC-16 in Lin et al., 2012) these are not included under the umbrella of aPN1. Similarly, the aPN(GCI) driver used here shows expression in both the canonical GCI neurons [S3], as well as the set of GABA-ergic interneurons that cofasciculate with these neurons; although these cell types are distinguishable by cell body size and neurotransmitter expression, they likely arise from the same lineage and may be co-expressed in many putative GCI drivers. In addition, should aLN(PCI) correspond to AMMC-IVLP PN2, it is likely better termed an aPN; more detailed clonal analysis of this line will be required to determine whether it shares a contralateral projection to IVLP, which is not obvious in GAL4-derived images. Some cell types in each study have no obvious correlates, which may be an

artifact of limited sampling, the reagents used in each study, or – for analysis of *fru*^{M}-expressing neurons – limited expression of *fru*^{M} (or the *fru*^{M} reporter) within a larger lineage of non-*fru*^{M}-expressing neurons.

Cell Type	***CRM Line***	***AMMC arbor***	***Off-target expression (Brain)***	***Off-target expression (VNC)***
aPN1	*R45D07*	*B*	*Possible ascending gustatory projection from foreleg? Very dim expression in WED neuron.*	*Minor innervation of each leg from periphery; possible minor expression in terminal abdominal nerve.*
	R63A03	*B*	*Giant fiber; ~4 posterior lineages with dim expression in ~6 cells each.*	*Leg nerves; paired single neurons with broad arborization in 1-3 thoracic neuropile; ~10 total other neurons.*
	R22B11	*B*	*5 distinct clusters in posterior brain ; olfPN(distal); medullary neurons or glia.*	*Perhaps ~12 neurons in the thoracic VNC; minor innervation of haltere nerve.*
	R59C10	*B*	*Large population of medullary neurons; ~6 neurons in posterior brain; minor expression in olfactory vPN lineage.*	*Expression in 6-8 lineages, with ~4-8 cells per lineage.*
aPN2	*R24C06*	*C/E*	*5 small cell bodies, possibly of aPN1 cell type; ~10 other neurons in SOG region; little expression in posterior brain.*	*Expression in 3 VNC clusters with ~4 cells per cluster; relatively dim.*
aPN3	*R70G01*	*C/E*	*Expression in one posterior cluster, likely the population of doublesex-expressingPC2 neurons of Robinett et al., 2010. Dim expression in 6 cells at dorsal protocerebrum.*	*None.*
	R30A07	*C/E*	*Minor expression in neurons innervating antennal lobe and SOG. Expression in central lineage innervating medulla and projecting to optic glomeruli of ventrolateral protocerebrum.*	*Expression in large neurons innervating the wing neuropile.*
aPN4	*R87G01*	*A*	*Expression in laminar neurons, as well as ~2 local AL neurons from the olfactory lPN lineage.*	*One neuron innervating the wing neuropile. Descending projections into the terminal abdominal nerve, from last abdominal segment.*
aPN5	*R12B10*	*A*	*Some expression in lamina and medulla, as well as minor expression in Kenyon cells of the mushroom body.*	*Expression in midline lineages of the first thoracic and abdominal segments, as well as segmental innervation of leg neuropile.*
	R37F03	*A*	*Some innervation of lateral horn (~4 neurons) and dorsal ventrolateral protocerebrum (~3 neurons).*	*Expression in first and third thoracic segments, as well as in neurons of the abdominal ganglia possibly projecting out of the terminal abdominal nerve.*
aLN (desc)	*R17A10*	*A/B*	*~4 neurons of ventral SOG innervating the median bundle.*	*~3 neurons innervating the first thoracic ganglion.*

			Some innervating of maxillary-labial nerve, but unclear whether this arises from the aLN(desc) lineage.	*Possible minor leg neuron expression.*
aPN (GF)	*R79D08*	*A*	*None.*	*None.*
aLN (al)	*R25B01*	*B*	*One neuron, innervating the medulla.*	*None.*
	R55C02	*B*	*None.*	*~3 cells innervating thoracic ganglia.*
aLN (am)	*R19E09*	*C/E*	*None.*	*~4 cells innervating thoracic ganglia.*
aLN (GCI)	*R11A07*	*A*	*None.*	*Expression in ~8 neurons in VNC.*
aLN (PCI)	*R51D11*	*A/WED*	*Expression in lobular neurons innervating optic tubercle, olfactory vPN and adPN lineage, paired large cells at ventral midline, and optic cleft innervation of WED.*	*Scattered expression through thoracic and abdominal ganglia.*
aLN (m)	*R52F05*	*A*	*~6 cells in the SOG that may correspond to other aLN cell types.*	*Several lineages within, including the terminal abdominal nerve.*

Table S3, related to Figure 1. CRM lines used to test the role of each cell type in this study. As off-target expression is crucial to the interpretation of behavioral experiments, we include a detailed description of any such expression in the CRM lines used in this study. Where available – and in particular, for the aPN1 and aLN(al) cell types that show behavioral phenotypes in the FR and SIL assays – we used several distinct CRM lines that had no overlap in this yRoff-target expression. Unless noted, no expression was observed in the terminal abdominal nerve, reflecting no innervation of ascending or descending projections from the genitalia. Significant sexual dimorphism in expression patterns was not observed at the level of gross morphology.

Male SIL: CRM-GAL4; UAS-shibireTS

CRM-GAL4 Line	n				mean SIL				STD(SIL)				p-value
	Control		Test		Control		Test		Control		Test		
	25°	30°	25°	30°	25°	30°	25°	30°	25°	30°	25°	30°	IX
R11A07	155	280	54	54	1.1	1.2	0.5	0.3	2.1	2.2	2	1.2	<0.5
R12B10	155	280	90	168	1.1	1.2	1.8	1.4	2.1	2.2	2.2	2.2	<0.2
R17A10	155	280	63	86	1.1	1.2	0.8	0.6	2.1	2.2	2.1	1.9	<0.5
R19E09	144	131	63	98	0.8	1.3	1.1	1.4	2	2.1	2.2	2.3	<0.7
R22B11	227	200	54	98	0.9	1.1	0.9	1.7	2.1	2.1	1.7	2.7	<0.3
R24C06	155	108	72	63	1.1	1.3	1.8	1.1	2.1	2.1	2.7	1.5	<0.07
R25B01	133	114	90	54	0.7	1.3	1.9	1.2	1.9	2	2.4	2.2	**<0.02**
R30A07	102	140	52	52	1.2	1.1	1.2	1.2	2.1	2.2	2.1	2.1	<0.8
R37F03	155	280	117	50	1.1	1.2	1.2	1.8	2.1	2.2	2.3	1.4	<0.3
R45D07	262	200	120	99	0.9	1.1	1.8	0.4	2.1	2.1	2.3	0.8	**<0.001**
R51D11	155	280	90	81	1.1	1.2	0.7	0.6	2.1	2.2	2.2	1.4	<0.6
R52F05	202	280	79	70	0.8	1.2	0.3	1.3	2.1	2.2	1.2	2.6	<0.2
R55C02	133	114	62	72	0.7	1.3	1.1	.7	1.9	2	2.2	1.9	**<0.02**
R59C10	262	200	72	142	0.9	1.1	1.7	1.1	2.1	2.1	2.7	1.7	**<0.03**
R63A03	262	200	54	117	0.9	1.1	1.1	0.5	2.1	2.1	2.7	1.3	**<0.03**
R70G01	155	280	81	90	1.1	1.2	1.4	1.1	2.1	2.2	2.2	1.7	<0.3
R79D08	155	280	90	54	1.1	1.2	1.1	1.1	2.1	2.2	2.1	2.4	<0.9
R87G01	155	280	117	97	1	1.2	2.2	1.7	2.1	2.2	2.7	2	<0.08

Female receptivity: CRM-GAL4; UAS-shibireTS (wild-type males)

CRM-GAL4 Line	n				exp(coefficient)			SE(Coefficient)			p-value
	Control		Test								
	25°	30°	25°	30°	Temp	GAL4	IX	Temp	GAL4	IX	IX
R11A07	168	300	72	72	1.0	0.7	1.6	0.2	0.1	0.3	<0.2
R12B10	168	300	48	132	0.0	-0.4	0.0	0.3	0.1	0.3	<0.9
R17A10	168	300	55	156	0.8	0.7	0.9	0.2	0.1	0.3	<0.7
R19E09	168	300	84	108	0.8	0.7	0.7	0.2	0.1	0.3	<0.3
R22B11	168	300	72	84	1.3	0.7	0.6	0.2	0.1	0.3	<0.03
R24C06	168	300	48	108	1.3	0.7	0.6	0.3	0.1	0.3	<0.2
R25B01	168	300	72	84	1.7	0.7	0.4	0.2	0.1	0.3	**<0.001**
R30A07	168	300	84	120	0.8	0.7	0.7	0.2	0.1	0.3	<0.3
R37F03	168	300	72	84	1.3	0.7	0.6	0.2	0.1	0.0	<0.07
R45D07	168	300	96	96	1.1	0.7	0.6	0.2	0.1	0.3	**<0.03**
R51D11	168	300	48	72	1.0	0.7	0.6	0.2	0.1	0.3	<0.07
R52F05	108	144	72	60	1.1	0.5	0.5	0.2	0.2	0.4	<0.07
R55C02	168	300	72	97	1.3	0.7	0.3	0.2	0.1	0.3	**<0.001**
R59C10	168	300	48	120	1.4	0.7	0.5	0.2	0.1	0.3	**<0.005**
R63A03	168	300	60	72	1.3	0.7	0.5	0.2	0.1	0.3	**<0.01**
R70G01	144	192	84	84	1.5	0.5	0.5	0.2	0.2	0.3	**<0.03**
R79D08	168	300	72	60	1.7	0.7	0.7	0.2	0.1	0.3	<0.4
R87G01	168	264	72	96	1.3	0.6	0.6	0.2	0.1	0.3	<0.09

Female receptivity: CRM-GAL4; UAS-dTrpA1 (wild-type males)

CRM-GAL4 Line	n				exp(coefficient)			SE(coefficient)			p-value
	Control		Test								
	22°	27°	22°	27°	Temp	GAL4	IX	Temp	GAL4	IX	IX
R11A07	108	155	60	48	1.2	0.9	1.1	0.2	0.2	0.3	<0.9
R12B10	108	155	154	108	1.1	0.9	1.2	0.2	0.2	0.2	<0.4
R17A10	108	155	132	120	1.0	0.9	0.9	0.2	0.2	0.2	<0.6
R19E09	108	155	121	132	1.1	0.9	0.9	0.2	0.2	0.2	<0.7
R24C06	108	155	60	72	1.4	0.9	1.1	0.2	0.2	0.3	<0.7
R45D07	108	155	96	108	1.3	0.9	0.1	0.2	0.2	0.3	**<0.001**
R52F05	108	155	72	84	0.8	0.9	1.3	0.2	0.2	0.3	<0.3
R55C02	108	155	84	96	1.0	0.9	0.5	0.2	0.2	0.3	**<0.01**
R59C10	108	155	72	144	1.0	0.9	0.4	0.2	0.2	0.3	**<0.001**
R70G01	108	155	84	131	0.9	0.9	1.1	0.2	0.2	0.2	<0.8
R79D08	108	155	60	84	1.2	0.9	0.6	0.2	0.2	0.3	<0.07
R87G01	108	155	72	48	1.5	0.9	0.9	0.2	0.2	0.3	<0.8

Female receptivity: CRM-GAL4; UAS-trpA1 (dewinged males)

CRM-GAL4 Line	n				exp(coefficient)			SE(coefficient)			p-value
	Control		Test								
	22°	27°	22°	27°	*Temp*	*GAL4*	*IX*	*Temp*	*GAL4*	*IX*	*IX*
R24C06	84	144	132	144	2.8	0.6	1.9	0.4	0.5	0.6	<0.3
R59C10	84	144	72	48	1.0	0.6	0.8	0.7	0.5	1.1	<0.9
R70G01	84	144	60	60	2.5	0.6	1.3	0.5	0.5	0.7	<0.7

Table S4, related to Figures 3-6. Summary data for all behavioral tests on aLN and aPN lines. For all data, behavioral tests of each line were spread over several testing sessions; only control data from the same period is included for analysis. For male SIL data, we report the sample size and the mean and standard deviation of the SIL response for each of the four conditions tested (25°/30°: permissive and restrictive temperatures; *CX/Test*: the empty-GAL4 control line BDPG4U and the identified CRM-GAL4 line). Significance was determined via the *genotype*temperature* interaction term (IX) of a two-way ANOVA; a significant result reflects the temperature-sensitive effect of *shibire^{TS}* expression in the neurons targeted by the CRM-GAL4, independent of the effect of genotype

or temperature alone. For female receptivity, we report for each combination of genotype and temperature the sample size and the estimated hazard function (as the exponentiated coefficient and standard error) for *temperature* (Temp), *genotype* (GAL4), and *temperature***genotype* interaction (IX) as derived from the two-way Cox Proportional Hazards ANOVA. The exponentiated coefficient is an estimate the multiplicative hazard rate (i.e., the multiplicative effect of a condition on the likelihood of mating) while holding all other variables constant. For example, in the R45D07/dtrpA1 experiment, the value exp(coeff) = 0.1 for the interaction term reflects that female R45D07/dtrpA1 tested at 27C are 10% as likely to mate as flies in other conditions - this effect is significant at $p<0.001$. For both male SIL and female receptivity, significant results (at $p<0.05$) are shown in bold.

Supplemental Experimental Procedures

Classification of candidate auditory interneuron lines Using data and images from the JFRC FlyLight project, we screened 6000 CRM-GAL4 lines to identify 288 CRM-GAL4 lines that showed expression in candidate auditory interneurons arborizing in the lateral and medial AMMC [S4-6]. From these, we identified 12 classes of neurons based on cell body location and morphology of their arborization pattern within the brain, and supplemented by the generation of single-lineage clones[S4-7]. Each class of interneuron was identifiable in an average of 14 CRM lines, suggesting broad coverage, and a subset was selected that maximized robust and specific on-target expression for behavioral manipulation.

Groups of neurons with a common morphology identifiable in multiple CRM lines were identified as a common cell type; in some cases the site of primary fasciculation was used to discriminate similar cell types as arising from distinct lineages. To our knowledge, all identified lineages in *Drosophila* have a single site of neuropile entry for their primary arborization. This categorization is therefore unlikely to split known lineages inappropriately, but may group distinct but morphologically similar cell types. The 12 cell types thus identified are summarized in Figure 1C, Figure S1, and Supplemental Table 1. The expression pattern of each CRM line, and correspondence of each cell type with previously identified *fruitless*-expressing neurons in the AMMC is shown in and Figure S2 and Supplemental Table 2.

Notably, aLN(GCI) contains the Giant Commissural Interneurons (GCIs) that

are electrically coupled to the Giant Fiber [S8, 9]. We also found 15+ GABAergic interneurons with small cell bodies that co-fasciculate with the GCI, that may play a role in the Giant Fiber pathway (Figure S2). We refer to both populations collectively as aLN(GCI).

Fly stocks and rearing Flies used for behavioral testing were collected within 12 hours of eclosion and entrained at 5-9d under a 12-hour L/D cycle; behavioral testing was performed between 5-10hr *zeitgeber* time.

For behavioral screening, CRM-GAL4 lines were crossed to either UAS-shibire^{TS} [S10] or UAS-dTrpA1{2} [S11] and tested as double-heterozygotes. The empty-GAL4 driver BDPG4U was used as a control; BDPG4U contains a GAL4 gene without an enhancer driving it, and shares a common genetic background with the other CRM lines tested; this driver shows no visible expression in the CNS when crossed to UAS-GFP constructs (data not shown) [S4, 5]. For intersectional experiments, GAL4 driver lines were crossed to eyFLP; UAS-frt-stop-frt-*shibire^{ts}*; the eyFLP reagent reliably restricts expression of *shibire^{TS}* to neurons within the eye/antennal disc [S12, 13]. This manipulation allows targeting of all nearly JONs (using the R61D08-GAL4 driver, which expresses broadly in nearly all chordotonal neurons) or of the subset of *fru^{M}-expressing* JONs along with other peripheral *fru^{M}* neurons (using *fru^{GAL4}*).

Flies expressing *shibire^{TS}* were reared to eclosion and entrained at 18±1C, and tested at permissive and restrictive temperatures of 25±1C and 29.5C ±1, respectively (the restrictive temperature is referred to as 30C in the figures). Flies expressing *dTrpA1* were reared and entrained at 21±1C and tested at permissive

and restrictive temperatures of 22±1C or 27 ±1C, respectively [S11, 14]. CS-Heisenberg (wild type) males used in female receptivity assays were reared and entrained at 25±1C. Male flies were entrained in groups of 10, and females in groups of 20.

Female receptivity Hearing in females was evaluated by observing the copulation latency (time to mating) of a female placed with a wild-type male fly in a cylindrical mating chamber (11mm diameter, 6mm height) [S15-17]. Male (CS-Heisenberg) and female flies were aspirated into opposite sides of the test chamber, separated by a transparent divider, and allowed to acclimatize at the test temperature for 15min. After removal of the divider, the latency to copulation was observed over a 20-minute window; this latency depends critically on antennal hearing [S18, 19].

In some experiments, the wings of male flies were removed at the first medial cross-vein using fine forceps, or the aristae of female flies were removed at the base. These amputations were performed 48-72 hours before behavioral testing to allow recovery. A minimum of 18 courting pairs were tested for dewinged and de-aristae'd manipulations. For *shibire*^{TS}, and *dTrpa1* manipulations, a minimum of 48 pairs was evaluated for each genotype, and test flies were compared to matched controls from the same day of testing.

SIL response The "Song Induced Locomotion" (SIL) assay builds on previous observations that male flies show a locomotor response to synthetic courtship song was observed by high-throughput video tracking [S19-23]. Briefly, same-sex

pairs were placed in cylindrical acrylic chambers (16mm diameter x 10mm height) with a nylon mesh floor (150μm spacing; Small Parts Inc., Seattle, WA) and incubated at the test temperature for 15 minutes. They were then moved to the test apparatus, and presented with synthetic courtship song (see below). Courtship song was presented via a NIDAQ 6229 interface (National Instruments, Austin, TX) and an A500 linear amplifier (Willich, Germany), driving a 12-inch subwoofer (D10G HiVi Woofer, Parts Express, Springboro, OH) located 11cm below the behavior chamber.

Synthetic courtship song (see below) was presented at 80dB Sound Pressure Level (SPL), as measured by a calibrated audiometer; for 260hz sound at 11cm distance, the near-field equation predicts a corresponding particle velocity (detectable by the drosophila antenna) of ~90dB sound particle velocity level (SPVL), which was confirmed with a particle-velocity microphone (Microflown Technologies, Arnhem, NL) [S24]. These values are within the expected range of *Drosophila* courtship song during close courtship [S25].

Fly activity was recorded (Stingray Firewire800 camera; Allied Vision Technologies GmBH, Stadtroda, Germany) under 880nm backlit illumination from spotlights reflected from the speaker head (Edmund Optics, Barrington NJ); audio presentation and video recording were synchronized using a modified version of the gVision software suite (http://gvision-hhmi.sourceforge.net). Fly locomotion was tracked for each chamber using a modified version of Ctrax, deployed in a high-throughput cluster environment (http://ctrax.sourceforge.net)[S26].

For analysis of the response to courtship song, the average speed of each pair of flies was calculated across a 5-minute period of silence followed by 5 minutes of continuous song presentation. From this raw data, a quantitative metric for the response to pulse song was calculated from aggregate speeds for each set of flies (grouped by sex, genotype and testing temperature) to generate an average SIL index as follows. The speed of each group of flies during the period of silence was fit to a slow exponential decay (of the form $s = ae^{-bt} + c$) representing gradual acclimatization to the test chamber. This exponential decay was used to generate a *predicted speed* for the following 5 minutes of song presentation, and the average difference between the *predicted* and *observed* speed during song presentation was designated as the SIL index. Using this index, pairs of wild-type male flies typically showed a 1-1.5mm/s increase in speed in response to song, while pairs of female flies showed a higher baseline but no significant difference between observed and expected speeds. At least 50 pairs were evaluated for each condition, and were paired with matched BDPG4U controls for date of testing (see Supplemental Table 4).

Synthetic song Synthetic pulse song was generated as a series of Gaussian-windowed pulses with a 260hz intrapulse frequency (IPF) and a half-width of 6ms, with bursts of 5 pulses presented at 30% duty cycle. Variant songs using other IPIs preserved the number of pulses within each burst as well as the burst duty cycle, and therefore varied in the duration of each burst. For “scrambled song” controls, IPIs within a burst were uniformly distributed between approximately 0 and 70ms.

Reports of IPFs in the literature vary widely [S27-35] and range from ~180hz [S36] to ~325hz. Our choice of a 260hz IPF was derived from [S31], and is near the median of reported values in the literature. Recordings from our Canton-S flies at 22C showed an IPF of 215hz, as calculated from a Welch spectrogram using a Hamming window, bin size of 512, and 10Khz sampling frequency. This method was capable of identifying the true IPF of our synthetic song (260hz) even when presented with a "scrambled" song control (IPIs ranging uniformly from 0-70ms) with an additional 20% additive white noise. With an increase in IPF of ~10hz per 1C, we expect the IPF of our synthetic song to be well matched at the restrictive temperatures used in our behavioral assays (27C and 29C, respectively) [S37].

The IPI of courtship song also varies with temperature, which provides a potential confound for temperature-sensitive genetic manipulations such as *shibire^{TS}* [S38]. Lab strains have previously shown an IPI of ~35ms at 27C, and are not expected to vary by more than 3ms from this baseline at restrictive temperatures [S39].

Histology Expression of CRM lines was visualized in 1-5 day-old progeny of CRM-GAL4 males crossed to p{JFRC2}*attP2*[4]. Overlap with *fru^{M}* expression was visualized in the male progeny of a cross between CRM-GAL4 males and *P{lexO-stingerGFP}; p{UAS-dsRed}, fru$^{P1.LexA}$* or *p{lexAop-FLP},p{UAS-frt-stop-frt-GFP}; fru$^{P1.\ LexA}$* females [S40-41]. dBrainbow clones were visualized in male progeny of a cross between CRM-GAL4 males and *hsCre;;UAS-dBrainbow,* raised at 22C without heat shock [S7].

Whole brain registration was performed using the VAA3D software suite (http://www.vaa3d.org)[S42]. Neuronal polarity was visualized by crossing CRM-GAL4 males to *p{UAS-SYT::HA}, {UAS-DSCAM::GFP}* [S43]. Brains were stained as described using mouse anti-*bruchpilot* (NC82, 1:20, DSHB), anti-*myc* (9E10, DSHB, 1:50), and anti-DsRed (PM005, 1:4000 Clontech); rabbit anti-GABA (A2052, 1:1000, Sigma), anti-GFP (A11029, 1:800, Invitrogen) and anti-mCD8 (Caltag, 1:600); and rat anti-HA (11867423001, 1:100, Roche)[S4]. Secondary antibodies included goat anti-rabbit Alexa-Fluor 488 (A11034; Invitrogen), goat anti-mouse Alexa-Fluor 430 (A11063), 568 (A11031), 633 (A21052) and 647 (A21236), as well as anti-rat Alexa-Fluor 633 (A21094) and 647 (A-21247); all secondary anitbodies were used at 1:500-1:1000. Images are representative of at least three samples.

GCaMP recordings GCaMP recordings in the aPN1 cell type were performed by 1-photon confocal microscopy at 488nm using a Zeiss 710 confocal microscope, and sampled at 13hz at a resolution of 128*128 pixels across a single plane. Female flies homozygous for w; p{10x-UAS-*GCaMP3}attp40; p{*R45D07-GAL4*}attP2* were prepared as described; the R45D07-GAL4 driver expresses bilaterally in ~12-15 aPN1 neurons with the canonical morphology[S12, 44]. For each recording, a female fly was cold-anesthetized and fixed into a small hole in a plastic plate with the proboscis facing up, and body and legs were stabilized with dental wax. The proboscis was removed to expose the ventral brain, and bathed in hemolymph solution (103mM NaCl, 5mM HEPES, 8mM trehalose, 10mM glucose, 26mM $NaHCO_3$, 1mM NaH_2PO_4, 2mM $CaCl_2$, and 1.5mM $MgCl_2$).

Synthetic song stimuli were delivered from a speaker 20cm distant, calibrated to 90dB SPVL for 35ms pulse song stimuli, as measured by a Microflown sensor (Microflown Technologies, Arnhem, NL). This stimulus corresponded roughly to the recorded amplitude of courtship song at ~5mm distance. Recordings from the right AMMC and WED of six flies were used for analysis; data from one other fly was discarded because AMMC and WED signals were not correlated, likely a result of movement artifacts.

ROI selection and ΔF/F calculation from the GCaMP3 signal were generated from six flies, using by custom software written in Matlab (The Mathworks, Inc; Natick, MA). For pulse song stimuli, $\Delta F/F$ was calculated as the peak GCaMP response following the stimulus minus the mean of a 1.3-2.6 second pre-stimulus period, and normalized by baseline fluorescence for the entire set of trials.

Statistical methods For female receptivity assays, copulation latency follows a survival model. For genetic manipulations, we sought to test for the specific effect of temperature-sensitive neuronal silencing or hyperactivation on copulation latency, while accounting for the nonspecific effects of genotype or temperature alone. We calculated this effect as a significant Wald test for *genotype x temperature interaction* in a two-way Cox Proportional Hazard ANOVA model, using the *survival* package in R, followed by evaluation of the mating hazard ratio (see also Supplemental Table 4; http://www.r-project.org). The *p* value for this interaction term is reported in the main text and figure legends; note that the effect of temperature or genotype alone are independent of this interaction term,

and are not strictly interpretable in the presence of a significant *temperature*genotype* interaction.

For male song-induced locomotion (SIL), a statistically significant disruption in courtship hearing was identified by two-way ANOVA. We tested for a significant *genotype* x *temperature* interaction, independent of the effect of genotype or temperature alone. We noted some deviation from normality for SIL data; however, the F-test is robust to these deviations for large N. The significance of the ANOVA interaction term is reported in the text and figures, and detailed in Supplemental Table 4.

For ease of visualization, the SIL index is presented in reduced form, as the response at restrictive temperature for each genotype, normalized by the response at permissive temperature (ie., $SIL_{29.5C}$ / SIL_{25C}). Values less than 1 reflect genotype-specific decreases in the SIL response at restrictive temperatures, while p-values represent the significance of the *genotype x temperature* interaction. While we present this reduced form in the figures for ease of visualization, we note that it is not strictly comparable to the ANOVA calculation, and therefore include a full data table for all aLN/aPN behavioral data in Supplemental Table 4.

For GCaMP analysis, we observed that ΔF/F responses showed an approximately normal distribution, as determined by the Jarque-Bera test, and were analyzed accordingly. For comparison of AMMC and WED responses in Figure 7 and Figure S2, linear and nonlinear fits were calculated in Matlab by Total Least Squares regression using the TLS package [S45]. P-values for significant linear and nonlinear fits were derived from a significant reduction in

residual variance by comparison to the group mean and the best linear fit, respectively, and calculated by F-test.

Supplemental References

S1. Lai, J. S.-Y., Lo, S.-J., Dickson, B. J., and Chiang, A.-S. (2012). Auditory circuit in the Drosophila brain. Proc Natl Acad Sci US A *109*, 2607–2612.

S2. Lin, S., Kao, C.-F., Yu, H.-H., Huang, Y., and Lee, T. (2012). Lineage Analysis of Drosophila Lateral Antennal Lobe Neurons Reveals Notch-Dependent Binary Temporal Fate Decisions. Plos Biol *10*, e1001425.

S3. Strausfeld, N. J., and Bassemir, U. K. (1983). Cobalt-coupled neurons of a giant fibre system in Diptera. J Neurocytol *12*, 971–991.

S4. Pfeiffer, B. D., Ngo, T. T. B., Hibbard, K. L., Murphy, C., Jenett, A., Truman, J. W., and Rubin, G. M. (2010). Refinement of Tools for Targeted Gene Expression in Drosophila. Genetics *186*, 735–755.

S5. Pfeiffer, B. D., Jenett, A., Hammonds, A. S., Ngo, T.-T. B., Misra, S., Murphy, C., Scully, A., Carlson, J. W., Wan, K. H., Laverty, T. R., et al. (2008). Tools for neuroanatomy and neurogenetics in Drosophila. Proc Natl Acad Sci US A *105*, 9715–9720.

S6. Jenett, A., Rubin, G. M., Ngo, T.-T. B., Shepherd, D., Murphy, C., Dionne, H., Pfeiffer, B. D., Cavallaro, A., Hall, D., Jeter, J., et al. (2012). A GAL4-Driver Line Resource for Drosophila Neurobiology. Cell Reports *2*, 991–1001.

S7. Hampel, S., Chung, P., McKellar, C. E., Hall, D., Looger, L. L., and Simpson, J. H. (2011). Drosophila Brainbow: a recombinase-based fluorescence labeling technique to subdivide neural expression patterns. Nature Methods *8*, 253–259.

S8. Johnston, C. (1855). Auditory Apparatus of the Culex Mosquito (J. micr. Soc. OS).

S9. Nadrowski, B., Effertz, T., Senthilan, P. R., and Göpfert, M. C. (2011). Antennal hearing in insects--new findings, new questions. Hear. Res. *273*, 7–13.

1S0. Kitamoto, T. (2001). Conditional modification of behavior in Drosophila by targeted expression of a temperature-sensitive shibire allele in defined neurons. Journal of Neurobiology *47*, 81–92.

S11. Hamada, F. N., Rosenzweig, M., Kang, K., Pulver, S. R., Ghezzi, A., Jegla, T. J., and Garrity, P. A. (2008). An internal thermal sensor controlling temperature preference in Drosophila. Nature *454*, 217–220.

S12. Yorozu, S., Wong, A., Fischer, B. J., Dankert, H., Kernan, M. J., Kamikouchi, A., Ito, K., and Anderson, D. J. (2009). Distinct sensory

representations of wind and near-field sound in the Drosophila brain. Nature *458*, 201–205.

S13. Stockinger, P., Kvitsiani, D., Rotkopf, S., Tirián, L., and Dickson, B. J. (2005). Neural circuitry that governs Drosophila male courtship behavior. Cell *121*, 795–807.

S14. Rosenzweig, M. (2005). The Drosophila ortholog of vertebrate TRPA1 regulates thermotaxis. Genes and Development *19*, 419–424.

S15. Manoli, D. S., Foss, M., Villella, A., Taylor, B. J., Hall, J. C., and Baker, B. S. (2005). Male-specific *fruitless* specifies the neural substrates of *Drosophila* courtship behaviour. Nature *436*, 395–400.

S16. Manoli, D. S., and Baker, B. S. (2004). Median bundle neurons coordinate behaviours during Drosophila male courtship. Nature *430*, 564–569.

S17. Kitamoto, T. (2002). Conditional disruption of synaptic transmission induces male-male courtship behavior in Drosophila. Proc. Nat. Acad. Sci. *99*, 13232–13237.

S18. Bastock, M., and Manning, A. (1955). The courtship of Drosophila melanogaster. Behaviour *8*, 85–111.

S19. Crossley, S. A., Bennet-Clark, H. C., and Evert, H. T. (1995). Courtship song components affect male and female Drosophila differently. Animal Behaviour *50*, 827–839.

S20. Schilcher, von, F. (1976). The role of auditory stimuli in the courtship of Drosophila melanogaster. Animal Behaviour *24*, 18–26.

S21. Eberl, D., Duyk, G., and Perrimon, N. (1997). A genetic screen for mutations that disrupt an auditory response in Drosophila melanogaster. Proceedings of the National Academy of Sciences of the United States of America *94*, 14837.

S22. Schilcher, von, F. (1976). The function of pulse song and sine song in the courtship of Drosophila melanogaster. Animal Behaviour *24*, 622–625.

S23. Kamikouchi, A., Inagaki, H. K., Effertz, T., Hendrich, O., Fiala, A., Göpfert, M. C., and Ito, K. (2009). The neural basis of Drosophila gravity-sensing and hearing. Nature *458*, 165–171.

S24. de Bree, H., Svetovoy, V., and Raangs, R. (2004). The very near field; theory, simulations and measurements of sound pressure and particle velocity in the very near field. ICSV11.

S25. Bennet-Clark, H. C. (1971). Acoustics of insect song. Nature 234, 255 - 259.

S26. Branson, K., Robie, A. A., Bender, J., Perona, P., and Dickinson, M. H. (2009). High-throughput ethomics in large groups of Drosophila. Nature Methods *6*, 451–457.

S27. Ewing, A., and Bennet-Clark, H. (1968). The courtship songs of Drosophila. Behaviour *31*, 288–301.

S28. Cowling, D., and Burnet, B. (1981). Courtship songs and genetic control of their acoustic characteristics in sibling species of the Drosophila melanogaster subgroup. Animal Behaviour *29*, 924–935.

S29. Villella, A., Ryner, L., and Baker, B. (1994). Behavioral and neurobiological implications of sex-determining factors in Drosophila - Taylor - 2005 - Developmental Genetics - Wiley Online Library. Developmental ….

S30. Villella, A., and Hall, J. C. (1996). Courtship anomalies caused by doublesex mutations in Drosophila melanogaster. Genetics *143*, 331–344.

S31. Villella, A., Gailey, D. A., Berwald, B., Ohshima, S., Barnes, P. T., and Hall, J. C. (1997). Extended reproductive roles of the fruitless gene in Drosophila melanogaster revealed by behavioral analysis of new fru mutants. Genetics *147*, 1107–1130.

S32. Ritchie, M. G., and Kyriacou, C. P. (1996). Artificial selection for a courtship signal in Drosophila melanogaster. Animal Behaviour *52*, 603–611.

S33. Rybak, F., Aubin, T., Moulin, B., and Jallon, J. (2002). Acoustic communication in Drosophila melanogaster courtship: Are pulse-and sine-song frequencies important for courtship success? Can. J. Zool. 80(6):987-996.

S34. Talyn, D., and Dowse, H. (2004). The role of courtship song in sexual selection and species recognition by female. Animal Behaviour *68*, 1165–1180.

S35. Wheeler, D. A., Fields, W. L., and Hall, J. C. (1988). Spectral analysis of Drosophila courtship songs: D. melanogaster, D. simulans, and their interspecific hybrid. Behav Genet *18*, 675–703.

S36. Riabinina, O., Dai, M., Duke, T., and Albert, J. T. (2011). Active process mediates species-specific tuning of Drosophila ears. Curr Biol *21*, 658–664.

S37. Hoikkala, A., Aspi, J., and Suvanto, L. (1998). Male courtship song frequency as an indicator of male genetic quality in an insect species, Drosophila montana. Proceedings of the Royal Society B: Biological Sciences *265*, 503–508.

S38. Shorey, H. H. (1962). Nature of the Sound Produced by Drosophila melanogaster during Courtship. Science *137*, 677–678.

S39. Pan, Y., Robinett, C. C., and Baker, B. S. (2011). Turning males on: activation of male courtship behavior in Drosophila melanogaster. PLoS ONE *6*, e21144.

S40. Meissner, G. W., Manoli, D. S., Chavez, J. F., Knapp, J. M., Lin, T. L., Stevens, R. J., Mellert, D. J., Tran, D. H., and Baker, B. S. (2011). Functional Dissection of the Neural Substrates for Sexual Behaviors in Drosophila melanogaster. Genetics *189*, 195–211.

S41. Lai, S.-L., and Lee, T. (2006). Genetic mosaic with dual binary transcriptional systems in Drosophila. Nat Neurosci *9*, 703–709.

S42. Peng, H., Chung, P., Long, F., Qu, L., Jenett, A., Seeds, A. M., Myers, E. W., and Simpson, J. H. (2011). BrainAligner: 3D registration atlases of Drosophila brains. Nature Methods *8*, 493–500.

S43. Cachero, S., Ostrovsky, A. D., Yu, J. Y., Dickson, B. J., and Jefferis, G. S. X. E. (2010). Sexual dimorphism in the fly brain. Curr Biol *20*, 1589–1601.

S44. Tian, L., Hires, S. A., Mao, T., Huber, D., Chiappe, M. E., Chalasani, S. H., Petreanu, L., Akerboom, J., Mckinney, S. A., Schreiter, E. R., et al. (2009). Imaging neural activity in worms, flies and mice with improved GCaMP calcium indicators. Nature Methods *6*, 875–881.

S45. Petráš, I., and Bednárová, D. (2010). Total Least Squares Approach to Modeling: A Matlab Toolbox. Acta Montanistica Slovaca *15*.